Korean J. Chem. Eng., 34(3), 664-671 (2017)
DOI: 10.1007/s11814-016-0299-8

pISSN: 0256-1115
eISSN: 1975-7220

Effect of acid sites on catalytic destruction of trichloroethylene over solid acid catalysts

Tiantian Wang*, Qiguang Dai,†, and Fuwu Yan*,†**

*Hubei Key Laboratory of Advanced Technology for Automotive Components & Hubei Collaborative Innovation Center for Automotive Components Technology, Wuhan University of Technology, Wuhan 430070, P. R. China
**Key Lab for Advanced Materials, Research Institute of Industrial Catalysis, School of Chemistry & Molecular Engineering, East China University of Science and Technology, Shanghai 200237, P. R. China
(*Received 5 May 2016 • accepted 24 October 2016*)

Abstract−The catalytic destruction of trichloroethylene (TCE) over several solid acid catalysts (HZSM-5, γ-Al_2O_3 and SBA-15/P) was evaluated under dry conditions. The activity order was found to be: HZSM-5>SBA-15/P>γ-Al_2O_3. It was reported that Brønsted and Lewis acid sites of catalysts both played an important role on TCE catalytic destruction, while the Brønsted acid sites were more decisive. Additionally, the formation of the polychlorinated by-product (tetrachloroethylene, PCE) over HZSM-5 and γ-Al_2O_3 catalysts was observed and attributed to the presence of Lewis acid sites and basic O^{2-}, and PCE was not detected over SBA-15/P catalyst due to the presence of only Brønsted acid sites. The TCE/O_2-TPSR studies demonstrated that the main oxidation products during TCE catalytic destruction are CO, CO_2 and Cl_2, and the carbon in TCE was firstly converted to CO and then further oxidized into CO_2 by gas phase O_2.

Keywords: Trichloroethylene, CVOCs, Catalytic Oxidation, Polychlorinated Byproducts, Molecular Sieve

INTRODUCTION

Chlorinated volatile organic compounds (CVOCs) are released directly to the atmosphere in the form of flue gases in a variety of industrial processes, such as the manufacture of vinyl chloride, herbicides, plastics and solvents, and metal degreasing processes. Such compounds are hazardous to human health due to their high toxicity and recalcitrance; moreover, some lead to the destruction of ozone layer and global warming. So, their industrial emissions have been restricted by environmental protection laws of many countries, and the remediation of CVOCs is important and necessary. Catalytic destruction/combustion has been considered as an effective and economical strategy for CVOCs elimination due to its low operating temperature (300-500 °C), high efficiency for low concentration of CVOCs and the potential selectivity towards the formation of harmless reaction products.

The development of catalysts for (C)VOCs catalytic destruction/combustion is vital, and most of the previous works are focused on the development of two types of catalysts: noble metals and transition metal oxides. Noble metal catalysts [1-5] have been claimed to be highly active in the destructive oxidation of (C)VOCs, but may be susceptible to deactivation by HCl and Cl_2 produced during the destruction reaction and the formation of polychlorinated by-products due to the presence of Cl_2 as well. Another option, transition metal oxide based catalysts [6-16], are generally more resistant to the deactivation of chlorine poisoning, but conversely with lower catalytic performance. Among transition metal oxide catalysts, chromium-based catalyst is an exception and exhibits the highest activity for CVOCs catalytic destruction [13,17]. Although very active, the application of this catalyst is restricted to low operation temperatures owing to the formation of volatile and very toxic chromium oxychloride [18]. More recently, solid acid catalysts as a third type of catalysts, including protonic zeolites (such as H-Y, H-MOR and HZSM-5), alumina and alumina-based composite oxides, have been proposed for CVOCs catalytic destruction [19-26]. It is well accepted in the literature [27-29] that oxidation of CVOCs over acidic supports and/or catalysts is initiated by the adsorption and dissociation of the chlorinated hydrocarbons on the Brønsted acidic sites. The activity is associated with the number and strength of Brønsted acid sites. Studies evidenced that not the total acidity but the modest concentration of strong Brønsted acidic sites had a dominant effect on catalytic performance for CVOCs destruction [24]. However, less consideration was given the roles of Lewis acidic sites in CVOCs catalytic destruction, for example, the effects on catalytic activity and chlorinated by-products distribution. Well-known, Brønsted and Lewis acidic sites usually are coexistent in traditional zeolite solid acid catalysts; thus, it is important to precisely determine the sole role of these two acid sites.

Recently, SBA-15 mesoporous molecular sieves have attracted increasing attention due to larger pore size, thicker pore wall and higher hydrothermal/thermal stability, which make them one of the most promising catalytic materials, especially as carriers for active species. It is well known that purely siliceous SBA-15 only shows very low catalytic activity, even almost not any activity, due to the absence of heteroatom or acid active sites. However, abundant and high active surface hydroxyl group existing in SBA-15 makes the modification (such as anchoring, grafting) of surface properties possible and various active sites are generated [30,31], which lets the modified SBA-15 be used widely as catalytic materials. Additionally, because of the low, even no, activity of purely siliceous SBA-

†To whom correspondence should be addressed.
E-mail: daiqg@ecust.edu.cn, yanfuwu@vip.sina.com

15, surface properties (such as surface acidity and redox properties) generated through the modification treatments are definite, which makes the understanding of the roles of surface properties and reaction mechanism easier and clearer. Herein, surface acidic properties of purely siliceous SBA-15 are adjusted controllably by the methods reported in the literature [32], and the SBA-15/P samples only with Brønsted acid sites are prepared. The catalytic activity and selectivity for TCE catalytic destruction over three solid acid catalysts including HZSM-5 and γ-Al_2O_3 are investigated, and the roles of Brønsted and Lewis acid sites are discussed in detail.

EXPERIMENTAL

1. Catalysts Preparation

Purely siliceous SBA-15 mesoporous molecular sieves (designated here as Si-SBA-15) were prepared as follows: 9.4 mL of tetraethyl orthosilicate (TEOS) were added to 30 mL aqueous HCl solution (pH≈0.7). This solution was stirred for 3 h at 40 °C and then added to 63 mL aqueous HCl solution (pH≈0.7) containing 4 g triblock copolymer (EO20PO20EO20, Aldrich). After being stirred for 24 h, this mixture gel was transferred to a Teflon container and kept at 100 °C for 24 h. Then it was cooled to room temperature, the solid obtained was filtered, washed by anhydrous ethanol, dried at 120 °C overnight, and then calcined at 550 °C for 6 h in air to remove the template.

Surface phosphorus species were externally introduced onto the surface of purely siliceous SBA-15 by impregnation method to prepare acidic solid catalyst only with Brønsted acid sites according to the procedures given in the literature [32]. 1 g of Si-SBA-15 sample was impregnated into 4.5 mL of phosphoric acid solution. Then, the phosphoric acid impregnated SBA-15 sample was dried in the oven at 100 °C for 8 h and calcined at 550 °C for 3 h. By adjusting the concentration of phosphoric acid solution, the phosphorus-containing SBA-15 samples with Si/P=25 were prepared and designated here as SBA-15/P, and the BET surface area and average pore size was 623 m^2/g and 5.4 nm, respectively. Moreover, phosphorus modified SBA-15 with the Si/P ratio 12.5, 50 and 100 also were prepared and used for catalytic combustion of TCE to studied the effects of acid number.

As references, commercial HZSM-5 (Si/Al=50, Nankai University Catalyst Co., Ltd.) and γ-Al_2O_3 (Sinopharm Chemical Reagent Co., Ltd.) were used, the BET surface area was 354 and 208 m^2/g, and the average pore size was 0.6 and 12.8 nm, respectively.

2. Temperature Programmed Desorption (TPD)

TPD experiments of NH_3 and TCE were performed in a quartz micro-reactor attached with a gas chromatograph (GC) equipped with a thermal conductivity detector (TCD). 100 mg of sample was first loaded in the reactor and heated in flowing N_2 at 550 °C for 2 h to remove the H_2O and CO_2 adsorbed on the sample surface. NH_3 or TCE was then introduced to the reactor after it was cooled to 100 °C. To remove the weakly or physically adsorbed NH_3 or TCE, the sample was swept using flowing N_2 at 100 °C for 2 h. The TPD experiments were then carried out in flowing N_2 with a flow rate of 30 mL·min^{-1} from 100 °C to 550 °C at a linear heating rate of 10 °C·min^{-1}. The desorption of NH_3 or TCE was detected by a GC and quantified based on the integrated areas of the desorption peak.

3. Temperature-programmed Surface Reaction (TPSR)

TPSR experiments were performed in the same equipment as the catalytic activity tests. The catalyst (100 mg) was previously swept with pure Argon at 550 °C for 2 h and then cooled to 200 °C. For the reaction test, the feed composition was 0.5 vol% TCE, 21 vol% oxygen and balance of Argon, and the flow rate of reactant gases was 50 cm^3·min^{-1} by means of mass flow meter controller. The reaction temperature increased from 200 to 650 °C at a heating rate of 5 °C·min^{-1}. Effluent gases were detected by a mass spectrometer (Balzers QMS-200); the following mass-to-charge ratios (m/z) were used to monitor the concentrations of products and reactants: 95 (TCE), 28 (CO), 44 (CO_2), 70 (Cl_2), 36 (HCl) and 131 (PCE).

4. *In Situ* FTIR Spectra of Pyridine Adsorption

The *in situ* FTIR spectra characterizing the adsorption of pyridine on solid acid catalysts were recorded under vacuum using a Shimadzu FTIR-8700 spectrometer having a resolution of 2 cm^{-1}. 15 mg of sample was pressed at a pressure of 2 ton·cm^{-2} into a self-supported wafer (16 mm in diameter). Prior to the adsorption of pyridine, the sample was treated under vacuum (<10^{-5} mbar) at 400 °C for 1 h. After the sample was cooled to room temperature, pyridine vapor was admitted to the IR cell for 30 min. After saturation, the sample was degassed at 100 °C to ensure that there was no more physically adsorbed pyridine left. The spectra of adsorbed pyridine were then collected. Then, the temperature of the cell was increased from 100 to 300 °C, and the spectra of adsorbed pyridine were measured at 150, 200, 250 and 300 °C, respectively. Difference spectra were obtained by subtracting the spectrum of the dehydrated samples from those obtained after pyridine adsorption.

5. Catalytic Activity Measurement

Catalytic destruction reactions were in a continuous flow microreactor constituted of a U shaped quartz tube of 3 mm of inner diameter at atmospheric pressure. The catalyst (100 mg) was placed at the bottom of the reactor and the temperature was measured with a thermocouple, the flow rate through the reactor was set at 50 cm^3·min^{-1} by a mass flow controller and the gas hourly space velocity (GHSV) was maintained at 15,000 h^{-1}. The feed stream to the reactor was prepared by delivering the liquid TCE (1,000 ppm) by a syringe pump into dry air (dried by silica gel and 5A zeolite). The

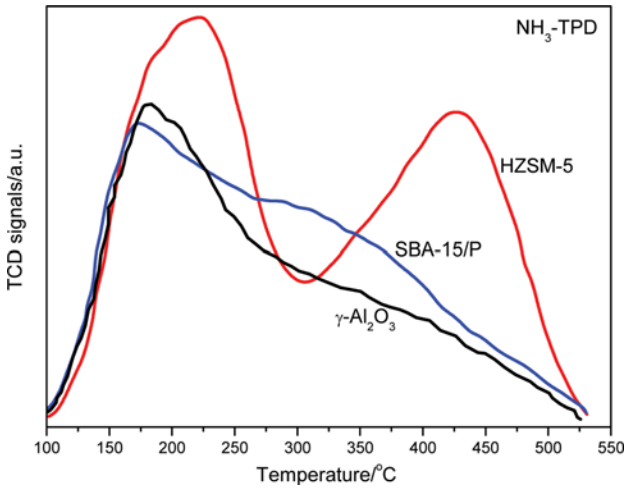

Fig. 1. NH_3-TPD profiles of different solid acid catalysts.

injection point was electrically heated to ensure complete evaporation of TCE. Gas samples were periodically taken from the flue exit gas, and the TCE conversions were measured on-line with a GC equipped with an electron capture detector (ECD).

RESULTS AND DISCUSSION

1. Characterization of Surface Acidic Properties

Two methods were used to characterize the acidic properties of the samples: (1) NH_3-TPD was used to analyze the number of the acid sites and the acid strength distribution of the samples, and (2) *in situ* FTIR spectra of pyridine adsorption were carried out to distinguish between Lewis (L) and Brønsted (B) acid sites.

The number and strength distribution of the acid sites present in the catalysts were investigated by NH_3-TPD analysis (Fig. 1) and the total acid amount also was listed in Table 1. In Fig. 1, the SBA-15/P sample shows a major desorption peak at about 175 °C, which is indicative of weak acid sites; moreover, a shoulder desorption

Table 1. The physicochemical properties and activity of SBA-15/P, Al_2O_3 and HZSM-5 catalysts

Catalysts	S_{BET} (m^2/g)	Average pore size (nm)	Total acid amount[a] (mmol/g)	B/L ratio[b]	TCE adsorption[c] (mmol/g)	TOF_{acid}[d] (10^{-3}/s)	TOF_{TCE}[e] (10^{-3}/s)
SBA-15/P	623	5.4	0.35	-	0.30	0.44	0.51
Al_2O_3	208	12.8	0.28	0	0.10	0.24	0.68
HZSM-5	354	0.6	0.55 (1.15)	3.15	0.13	0.34	1.44

[a]Total acid amount is measured based on NH_3-TPD results, the data in the parenthesis refer to LT/HT ratio

[b]The concentration of Brønsted acid and Lewis acid sites can be calculated from the integrated intensities of the $PyrH^+$ (1,540 cm^{-1}) and PyrL (1,450 cm^{-1}) peaks, and the ratio of L/B (Lewis acidity/Brønsted acidity) is calculated based on the data of Pyridine FT-IR at 200 °C

[c]TCE adsorption amount is measured based on TCE-TPD results

[d]The TOF_{acid} is obtained at 450 °C, and calculated based on the total acid amount

[e]The TOF_{TCE} is obtained at 450 °C, and calculated based on the TCE adsorption amount

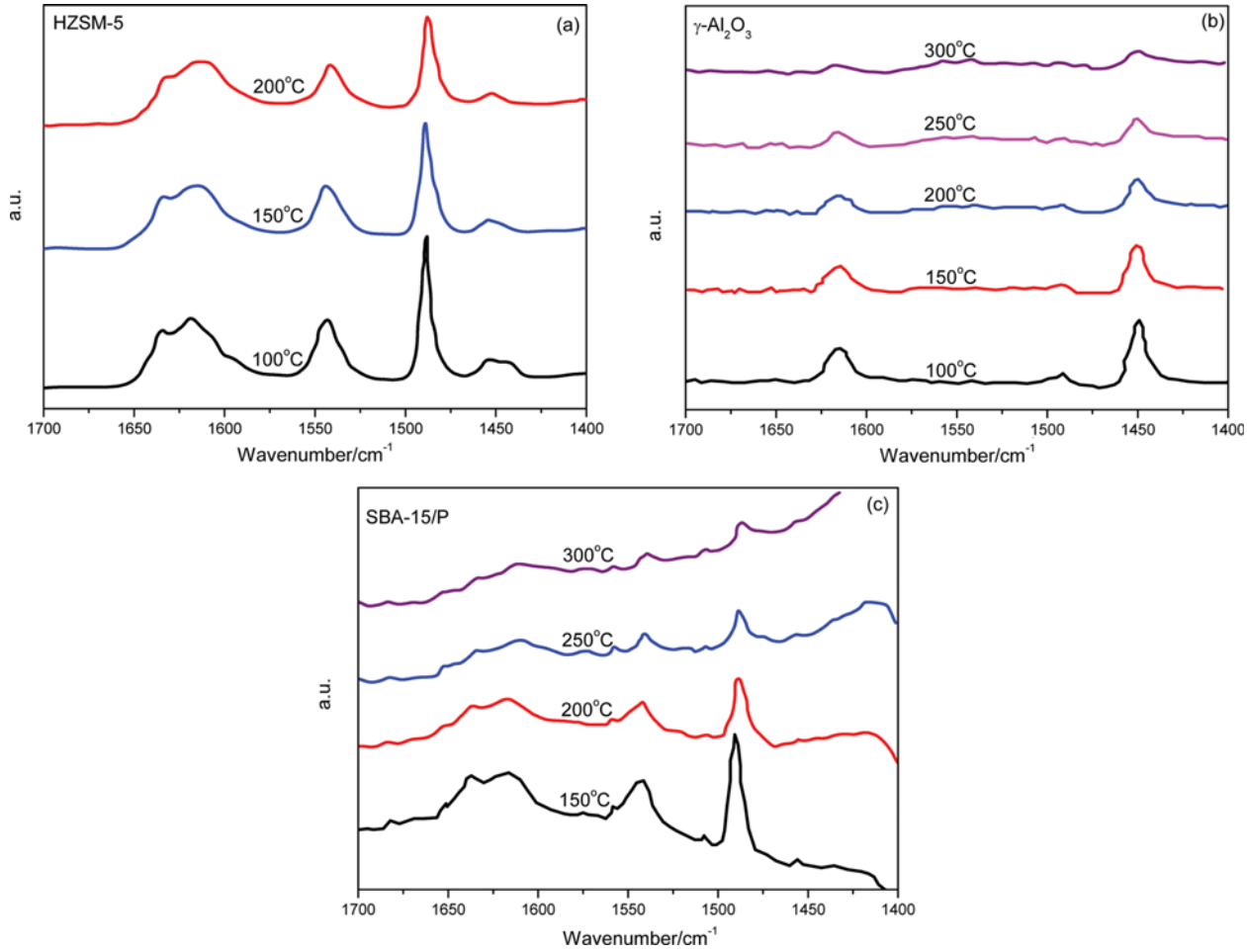

Fig. 2. *In situ* FTIR spectra of pyridine adsorption on different solid acid catalysts: (a) HZSM-5; (b) γ-Al_2O_3; and (c) SBA-15/P.

peak in the range of 300-450 °C also is observed. This result also confirms that the surface acidity of the modified SBA-15 samples can be substantially increased by simply grafting phosphorus species onto the Si-SBA-15, which is in accord with the literature results [32]. The γ-Al_2O_3 sample shows a typical broad peak with a major desorption peak around 175-185 °C. This wide NH_3 desorption peak of SBA-15/P and γ-Al_2O_3 samples indicates that the acid strength distribution of catalysts surface is uniform. The NH_3-TPD profile of HZSM-5 sample presents two sharp and symmetrical NH_3 desorption peaks; a major desorption peak around 225 °C, and the other smaller desorption peak was observed around 425 °C, which implies the presence of two types of acid sites (weak acid site at lower desorption temperature and medium-strong acid site). According to the integrated areas of the peak related to the total acid amount, HZSM-5 shows the largest total acid amount (0.55 mmol/g), with the ratio of weak and medium-strong acids around 1.15. Moreover, the amount of the total acid sites in SBA-15/P (0.35 mmol/g) is slightly higher than γ-Al_2O_3 sample (0.28 mmol/g).

Fig. 2 shows the *in situ* FTIR spectra of pyridine adsorption on the samples. All the samples show a band at 1,490 cm^{-1}, which can be assigned to pyridine associated with Brønsted or Lewis acid sites. Generally, the band at 1,445 cm^{-1} belongs to the adsorption of pyridine on Lewis acid sites (PyrL), and the band at 1,545 cm^{-1} is associated with the adsorption of pyridine on Brønsted acid sites ($PyrH^+$). As can be seen in Fig. 2, both types of acid sites are observed on HZSM-5 sample, and the ratio of B/L acid sites is about 3.15 (at 200 °C) according to the integrated areas of respective pyridine bands, which demonstrates that the HZSM-5 sample presents predominantly Brønsted acid sites with few Lewis acid sites. By contrast, only Lewis acid sites exist in γ-Al_2O_3 sample, which is widely accepted, while Brønsted acid sites are clearly present on the SBA-15/P sample without obvious Lewis acid sites, which indicates that the modification with phosphorous species on the surface of SBA-15/P will only lead to Brønsted acid sites. The same results were observed by Kawi [32], and they proposed reaction pathways that the generation of Brønsted acid sites from the grafted phosphorus species were formed from the dehydration of phosphoric acid which interacted with the hydroxyl groups of Si-SBA-15. According to the results of *in situ* FTIR spectra of pyridine adsorption, it can be confirmed that the acid sites presenting in these three catalysts are distinguishable, which would be favorable to investigate and understand the roles of different acid sits in catalytic destruction of TCE over these solid acid catalysts.

To investigate the adsorption of TCE on different acid sites and further understand the effect of acid sites on catalytic destruction of TCE, TCE-TPD studies were carried out. The result shown in Fig. 3 indicates that all catalysts show a strong desorption at 150-200 °C, and the desorption temperature of TCE on the SBA-15/P and γ-Al_2O_3 samples (180 °C) is lightly higher than on HZSM-5 sample (160 °C). Additionally, a shoulder desorption peak is observed for SBA-15/P sample at higher temperature range (325-450 °C). It can be found that the TCE-TPD of SBA-15/P and γ-Al_2O_3 samples are exactly similar with NH_3-TPD, but HZSM-5 sample shows distinct differences and presents only a sharp TCE desorption peak in low temperature ranges. Generally, the adsorption of TCE on solid acid catalysts should be ascribed to acid sites, especially Lewis

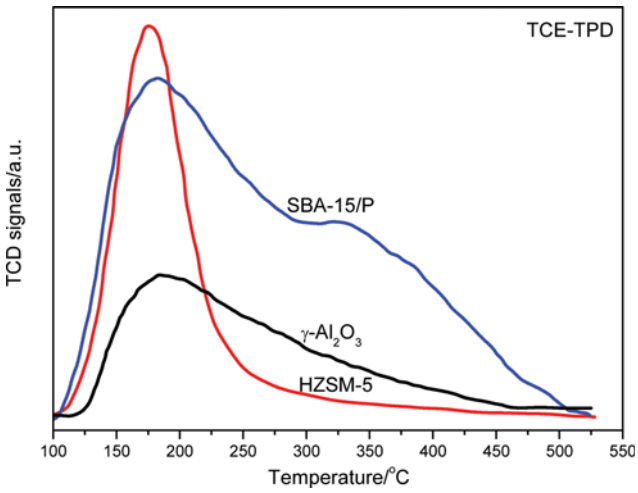

Fig. 3. TCE-TPD profiles of different solid acid catalysts.

acid sites, because the chlorinated ethylene molecule can be considered as a Lewis base [33]; thus, the results of TCE-TPD, including the number of desorption peaks and adsorption capacity, should coincide with NH_3-TPD. However, according to the desorption peaks area, the total amount of TCE desorption on the SBA-15/P sample is largest (0.3 mmol/g), which matches the number of acid sites (0.35 mmol/g); HZSM-5 (0.13 mmol/g) and γ-Al_2O_3 samples (0.1 mmol/g) present a lower TCE adsorption compared to NH_3-TPD. Generally known, ZSM-5 is a typical micro-porous zeolite with a straight channel of 5.4×5.6 Å and a sinusoidal channel of 5.1×5.5 Å, while the kinetic diameter of TCE molecule is 7.3 Å, which is bigger than the channel size of ZSM-5. This makes TCE molecules hard to access the channel of ZSM-5. Additionally, Brønsted acid sites of HZSM-5 are usually considered to be stronger than Lewis acid sites and mainly from the framework aluminum in microporous walls. Therefore, it can be inferred that the adsorption of TCE mainly occurs on the Lewis acid sites existing in the external surface of HZSM-5, which is attributed to the low TCE adsorption capacity and weak adsorption strength. Interestingly, TCE adsorption amount (0.13 mmol/g) is 23% total acid amount (0.55 mmol/g) and matches well with Lewis acid amount (B/L ratio is 3.15), while the external surface acid amount is usually about 10-20% total acid for the traditional HZSM-5. And for SBA-15 and γ-Al_2O_3, the pore size is large enough, the adsorption and diffusion of TCE on/in the pore is not subject to steric hindrance and thus displays a similar TCE-TPD curve with NH_3-TPD due to the adsorption of TCE that occurs on acid sites. While, the low TCE adsorption on γ-Al_2O_3 sample is ascribed to the weak adsorption strength of Lewis acid sites and weak basicity of TCE. Greene [33] suggested that the chlorinated ethylene can provide a lone pair of electrons and the catalysts as a Lewis acid which can accept the lone pair of electrons, so the catalytic activity of solid acid catalyst for catalytic oxidation of chlorinated ethylene lies in the adsorption strength of chlorinated ethylene on Lewis acid sites. But the adsorption strength of chlorinated ethylene is weak and could be weaker with the increase of chlorine atoms amount in chlorinated ethylene.

Combined with the results of *in situ* FTIR, it can be inferred that

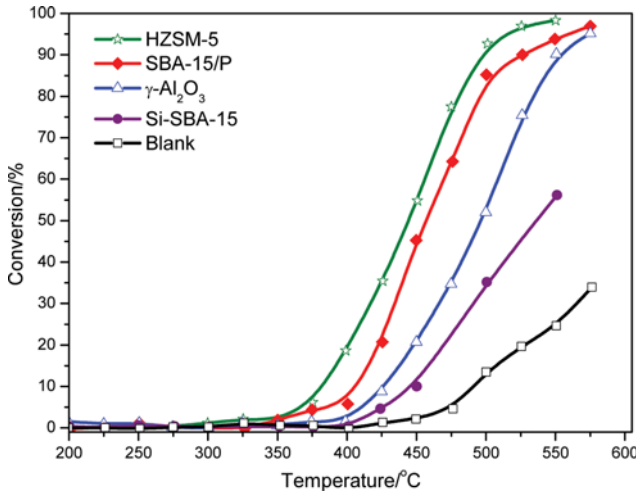

Fig. 4. The light-off curves for catalytic destruction of TCE over different solid acid catalysts.

TCE molecule as a Lewis base should be inclined to weakly adsorb on Lewis acid sites of solid acid catalysts *via* C=C double bonds, while the adsorption of TCE on Brønsted acid sites occurs between Cl and hydroxyl proton. Moreover, the activation and dissociation of C=C bond is more difficult than C-Cl bond due to the high dissociation energy of C=C bond, the presence of π-extended electron system and the adsorption strength of Lewis acid site. It also can be speculated that the Brønsted acid sites present better catalytic activity due to higher dissociation abilities.

2. Catalytic Activity Results

Fig. 4 shows the light-off curves of the catalytic destruction of TCE over three solid acid catalysts. A blank test placing just 0.3-0.5 mm crushed quartz glass into the reactor was also performed to check the extent of the reaction without any catalyst. The homogeneous destruction reaction occurs only above 425 °C and with conversion of 35% even at 575 °C. As shown in Fig. 4, the purely siliceous SBA-15 catalyst also shows a very low catalytic activity but slightly higher than the quartz glass, which indicates that abundant surface hydroxyl group of Si-SBA-15 is active due to its faint acid [34]. However, the SBA-15 sample modified by phosphorus species shows an evident higher catalytic activity: $T_{50\%}$ and $T_{90\%}$ are 450 °C and 510 °C, respectively; thus, the acid sites play a key role for the TCE catalytic destruction. In addition, the effect of H_3PO_4 loading on the catalytic activity also was investigated and the result is shown in Fig. 1S. The catalytic activity of SBA-15/P for TCE oxidation increases with the increase of H_3PO_4 loading due to the increase of acid sites, and the same results were reported by Wang et al. [35]. However, when the Si/P ratio is below 12.5, the framework structure and ordered mesopore of SBA-15 are partially destroyed, and the surface area also declines sharply. Thus, the Si/P ratio of 25 was adopted to evaluate the role of Brønsted acid for TCE oxidation. The common solid acid catalysts (HZSM-5 and γ-Al_2O_3) also show good catalytic performance for the catalytic destruction of TCE. In contrast, the catalytic activity order of TCE catalytic destruction over three different solid acid catalysts is: HZSM-5>SBA-15/P>γ-Al_2O_3. It is well accepted in the previous literature [27-29] that the medium-strong Brønsted acidic sites play a key role in determining the activity of acidic supports and/or catalysts since the oxidation of CVOCs is initiated by the adsorption of the hydrocarbons on these sites by proton transfer.

The *in situ* FTIR spectra of pyridine adsorption show that HZSM-5 and SBA-15/P possess many Brønsted acid sites, which brings up their better activity. However, compared with Si-SBA-15 or quartz glass, γ-Al_2O_3 with only Lewis acid sites presents significant catalytic activity for TCE catalytic destruction. Therefore, it can be inferred that the Brønsted and Lewis acid sites both play an important role in TCE catalytic destruction, but Brønsted acid sites are dominant. Tajima studied the decomposition of chlorofluorocarbons (CFCs) over a variety of solid acid catalysts [28], and suggested that γ-Al_2O_3 only with Lewis acid sites exhibited an obvious activity and CFCs seemed to be decomposed not only on the Brønsted acid site but also on the Lewis acid sites.

Besides the light-off curves to evaluate the catalytic performance of three catalysts, the activity also is further calculated based on per adsorption/-active site (such as acid site and TCE adsorption site) and listed in Table 1. The TOF_{acid} values (calculated based on the total acid amount) at 450 °C further confirmed that SBA-15/P (0.44×10^{-3} s^{-1}) and HZSM-5 (0.34×10^{-3} s^{-1}) samples with Brønsted acid sites display a better activity, while the relatively low TOF_{acid} of HZSM-5 is attributed to steric hindrance and the presence of Lewis acid sites with the lower activity. However, the TOF_{TCE} (calculated based on the TCE adsorption amount) reveals that SBA-15/P sample shows the worst performance probably due to the large surface area and the weaker strength of Brønsted acid sites compared with HZSM-5.

Additionally, a small amount of poly-chlorinated compounds such as tetrachloroethylene (PCE) as a by-product are detected over HZSM-5 and γ-Al_2O_3 catalysts, but the formation of PCE is not observed over SBA-15/P catalyst. Gonzalez-Velasco [4] also found that small amounts of PCE were generated during TCE catalytic destruction over ZSM-5, Y and MOR, and PCE peak concentration was slightly higher over H-Y zeolite than over HZSM-5 and H-MOR. The *in situ* FTIR spectra of pyridine adsorption showed that the amount of Lewis acid sites on H-Y was much greater than that of HZSM-5 and H-MOR, which indicated that the formation of PCE was closely correlated to Lewis acid sites. Feijen-Jeurissen et al. investigated the destruction mechanisms of TCE, and observed the formation of PCE [36]. They suggested that the formed by-product could be explained by chlorination followed by dehydrochlorination as follows (Scheme 1). Ballinger and Yates studied catalytic decomposition of 1, 1, 1-trichloroethane on high surface area alumina with Lewis acid ($A1^{3+}$) sites on surface and the by-product of CH_2=CCl_2 was formed *via* α, γ-HCl elimination at higher temperatures. They also claimed that the C-Cl bond of CH_3CCl_3 was linked to an $A1^{3+}$ site, while the C-H bond of the molecule associates with an O^{2-} site (base site, H abstraction must occur *via* a base) [37]. Additionally, Lewis acids catalysts (such as $FeCl_3$, $AlCl_3$, $SbCl_3$, $MnCl_2$, $MoCl_3$, $SnCl_4$ and $TiCl_4$) are usually used as principal catalysts for the preparation of chlorinated organic compounds

$$CCl_2{=}CHCl \xrightarrow{Cl_2} CCl_3\text{-}CHCl_2 \xrightarrow{\text{-HCl}} CCl_2{=}CCl_2$$

Scheme 1.

(including chlorinated alkanes and chlorinated aromatic hydrocarbons) in industry [38]. Therefore, it can be concluded that the coexistence of Lewis acid sites ($A1^{3+}$) and base sites ($Al\text{-}O^{2-}$) should be responsible for the formation of PCE during TCE catalytic destruction over HZSM-5 and γ-Al_2O_3 catalysts. Specifically, the C=C bond of TCE (as Lewis base) is activated and dissociated on Lewis acid sites and followed with chlorination by Cl_2 to form CCl_3CHCl_2 *via* an addition reaction; then E2 elimination reactions (HCl elimination) occur with the H abstraction by a basic O^{2-} and the C-Cl dissociation on Lewis acid sites. For SBA-15/P sample, due to the absence of basic O^{2-} and Lewis acid sites, the PCE by-product is not observed.

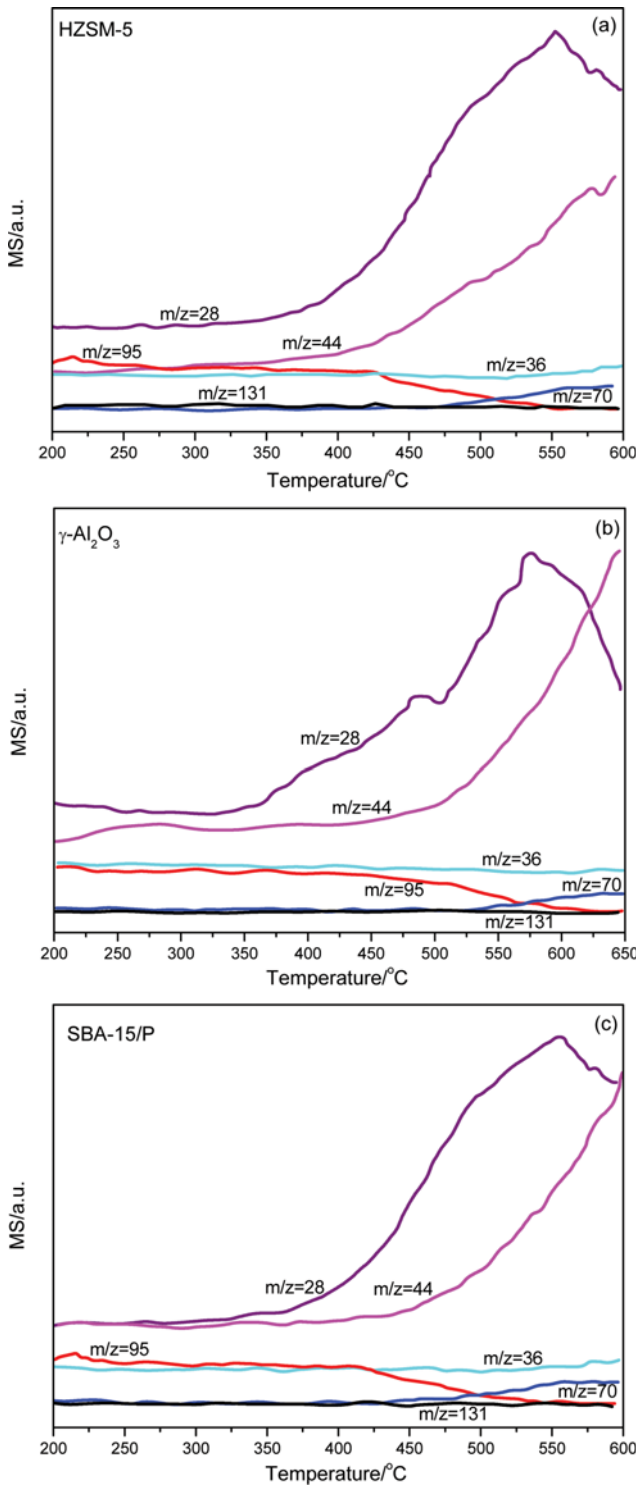

Fig. 5. TPSR curves for catalytic destruction of TCE over different solid acid catalysts: (a) HZSM-5; (b) γ-Al_2O_3; (c) SBA-15/P.

3. TCE/O_2-TPSR

Though the formation of PCE by-product is closely associated to basic O^{2-} and Lewis acid sites, the presence of Cl_2 is crucial as well. To confirm all the possible product formations (such as CO, CO_2, HCl, PCE and Cl_2), experiments of temperature programmed surface oxidation reaction of TCE (TCE/O_2-TPSR) were carried out and the results are presented in Fig. 5. First, it is essential to illustrate that the changes in intensity of the signals corresponding to HCl (36) and PCE (131) were not observed during TCE/O_2-TPSR over all catalysts, which are probably related to the detection sensitivity (lower limit of the mass spectrometer) and the low concentration or the strong adsorption on catalysts surface of HCl/PCE. The TCE/O_2-TPSR profiles of three solid acid catalysts show that the TCE ignites at about 425-450 °C, with $T_{90\%}$ value around 550 °C for HZSM-5 and SBA-15/P, while at 575 °C for γ-Al_2O_3 catalyst. The results coincide well with the light-off curves of TCE catalytic destruction. The formation of Cl_2 was detected over all catalysts once the destruction reaction occurred and the amount increased with the increasing of reaction temperature. The direct observation of Cl_2 provides an evidence that TCE can be chlorinated into CCl_3CHCl_2 by the addition reaction with the Cl_2 which can be *in-situ* generated from the oxidation of HCl or dissociated Cl species with O_2. Additionally, the relation of CO and CO_2 with the reaction temperature has attracted our special attention. As shown in Fig. 5, all the catalysts show signals attributed to CO (m/z=28) and CO_2 (m/z=44), and the CO formation reaches a maximum up to

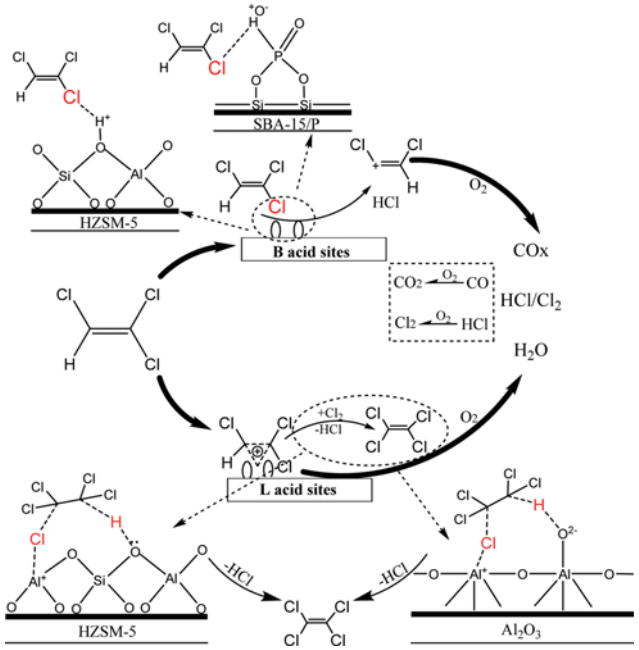

Scheme 2. The proposed mechanism of TCE catalytic destruction over HZSM-5, Al_2O_3 and SBA-15/P catalysts.

ca. 550-575 °C during the heating process. Compared to HZSM-5 and SBA-15/P, the CO formation peak temperature (T_p) on γ-Al_2O_3 catalyst shifts to higher temperature (T_p of HZSM-5 and SBA-15/P at ca. 550 °C and T_p of γ-Al_2O_3 at ca. 575 °C). In addition, the formation of CO_2 continuously increased for all catalysts. The CO formation with a maximum value and the continuous increase in the formation of CO_2 reveal that the carbon in TCE first is converted to CO and then fully oxidized by gas phase O_2 into CO_2 during TCE catalytic destruction over solid acid catalysts. The results also showed that the Brønsted acid sites (on HZSM-5 and SBA-15/P) are favorable to the further oxidation of CO into CO_2 at lower temperature. Based on experiments and comprehensive analysis, the process/mechanism of TCE catalytic destruction over three solid acid catalysts with different acid sites can be described by the following scheme (Scheme 2).

Additionally, the stability tests of three catalysts (HZSM-5, Al_2O_3 and SBA-15/P) also were performed at 450 °C and shown in Fig. 2S. All catalysts show an obvious deactivation in the initial stages (within 1 h); unsurprisingly, the coking deactivation is inevitable for solid acid catalysts during catalytic combustion of (C)VOCs. Moreover, the conversion of TCE on HZSM-5 displays a more rapid decline due to the presence of abundant micropore and strong Brønsted acid sites compared with the other two catalysts, and SBA-15/P almost presents the same stable conversion with HZSM-5 in the later stage. Although our results indicate that no further deactivation of all catalysts was observed in the short term (20 h), we speculate that the coking deactivation of catalysts will continue to happen over a prolonged period of time, while SBA-15/P also will show a better resistance to coking due to the presence of mesopore.

CONCLUSIONS

Three solid acid catalysts, SBA-15/P, γ-Al_2O_3 and HZSM-5, were evaluated for TCE catalytic destruction under dry conditions between 200 and 600 °C. The activity order was found to be: HZSM-5>SBA-15/P>γ-Al_2O_3, which coincided with the total acid amount, but the activity order per acid site was SBA-15/P>HZSM-5>γ-Al_2O_3. The *in situ* FTIR spectra of pyridine adsorption show that HZSM-5 has many Brønsted/Lewis acid sites but with weak Lewis acid sites (under 200 °C), while γ-Al_2O_3 has only Lewis acid sites, and only Brønsted acid sites were observed on SBA-15/P. These results demonstrate that both Brønsted acid sites and Lewis acid sites are active for TCE catalytic destruction, while Brønsted acid sites are more active (especially strong acid sites). For HZSM-5, the small pore size leads to significant mass-transfer issues, which limits the improvement of TCE destruction and due to the weak adsorption of TCE on HZSM-5 as well. Additionally, the formation of the byproduct PCE over HZSM-5 and γ-Al_2O_3 catalysts was attributed to Lewis acid sites and basic O^{2-} from Al_2O_3, and PCE was not observed over SBA-15/P due to absence of Lewis acid sites.

Although the solid acid catalysts present good activity for the catalytic destruction of TCE, the formation of the incomplete oxidation products CO and other polychlorinated by-products cannot be avoided. Thus, we consider that the transition metal oxide (such as CeO_2 or MnO_2) supported different solid acid materials would be a potential catalyst for the catalytic total oxidation of chlorinated hydrocarbons; however, the Lewis acid sites existing in solid acid supports should be avoided and inhibit the formation of polychlorinated by-products.

ACKNOWLEDGEMENTS

This work was supported by the National Natural Science Foundation of China (Nos. 21307033 and 21477036), and Shanghai Natural Science Foundation (No. 13ZR1411000).

SUPPORTING INFORMATION

Additional information as noted in the text. This information is available via the Internet at http://www.springer.com/chemistry/journal/11814.

REFERENCES

1. J. R. Gozalez, A. Aranzabal, J. I. Gutierrez-Ortiz, R. Lopez-Fonseca and M. A. Gutierrez-Ortiz, *Appl. Catal. B Environ.*, **19**, 189 (1998).
2. A. J. Aranzabal, L. Ayastuy-Arizti, J. R. Gonzalez-Marcos and J. R. Gonzalez-Velasco, *J. Catal.*, **214**, 130 (2003).
3. M. Kulazynski, J. G. van Ommen, J. Trawczynski and J. Walendziewski, *Appl. Catal. B Environ.*, **36**, 239 (2002).
4. X. L Liu, J. L. Zeng, J. Wang, W. B. Shi and T. Y. Zhu, *Catal. Sci. Technol.*, **6**, 4337 (2016).
5. J. E. Park, B. B. Kim and E. D. Park, *Korean J. Chem. Eng.*, **32**, 2212 (2015).
6. J. I. Gutierrez-Ortiz, R. Lopez-Fonseca, U. Aurrekoetxea and J. R. Gonzalez-Velasco, *J. Catal.*, **214**, 130 (2003).
7. X. D. Ma, M. Y. Zhao, Q. Pang, M. H. Zheng, H. W. Sun, J. Crittenden, Y. Y. Zhu and Y. S. Chen, *Appl. Catal. A*, **522**, 70 (2016).
8. Z. N. Shi, P. Yang, F. Tao and R. X. Zhou, *Chem. Eng. J.*, **295**, 99 (2016).
9. H. L. Greene, D. S. Prakash and K. V. Athota, *Appl. Catal. B Environ.*, **7**, 213 (1996).
10. G. A. Atwood, H. L. Greene, P. Chintawar, R. Rachapudi, B. Ramachandraan and C. A. Vogel, *Appl. Catal. B Environ.*, **18**, 51 (1998).
11. A. M. Padilla, J. Corella and J. M. Toledo, *Appl. Catal. B Environ.*, **22**, 107 (1999).
12. S. Cao, H. Q. Wang, F. X. Yu, M. P. Shi, S. Chen, X. L. Weng, Y. Liu and Z. B. Wu, *J. Colloid Interface Sci.*, **463**, 233 (2016).
13. P. Yang, S. F. Zuo, Z. N. Shi, F. Tao and R. X. Zhou, *Appl. Catal. B Environ.*, **191**, 53 (2016).
14. B. Ramachandran, H. L. Greene and S. Chatterjee, *Appl. Catal. B Environ.*, **8**, 157 (1996).
15. Y. P. Ren, A. D. Tang, L. Q. Hu and H. Xiang, *RSC Adv.*, **6**, 46822 (2016).
16. S. W. Jeon, J. E. Lee and J. K. Park, *Korean J. Chem. Eng.*, **32**, 230 (2015).
17. C. R. Rachapudi, P. S. Chintawar and H. L. Greene, *J. Catal.*, **185**, 58 (1999).
18. K. E. Jeong, D. C. Kim and S. K. Ihm, *Catal. Today*, **87**, 29 (2003).
19. R. Lopez-Fonseca, A. Aranzabal, J. I. Gutierrez-Ortiz, J. I. Alvarez-

Uriarte and J. R. Gonzalez-Velasco, *Catal. Today*, **87**, 29 (2003).
20. P. F. Sun, W. L. Wang, X. X. Dai, X. L. Weng and Z. B. Wu, *Appl. Catal. B Environ.*, **198**, 389 (2016).
21. S. X. Bai, B. B. Shi, W. Deng, Q. G. Dai and X. Y. Wang, *RSC Adv.*, **5**, 48916 (2015).
22. B. de Rivas, C. Sampedro, R. López-Fonseca, M. A. Gutiérrez-Ortiz and J. I. Gutiérrez-Ortiz, *Appl. Catal. A Gen.*, **417-418**, 93 (2012).
23. T. K. Tseng, L. Wang, C. T. Ho and H. Chu, *J. Hazard. Mater.*, **178**, 1035 (2010).
24. Q. Q. Huang, X. M. Xue and R. X. Zhou, *J. Mol. Catal. A Chem.*, **331**, 130 (2010).
25. M. Guillemot, J. Mijoin, S. Mignard and P. Magnoux, *Microporous. Mesoporous. Mater.*, **111**, 334 (2008).
26. M. E. Swanson, H. L. Greene and S. Qutubuddin, *Appl. Catal. B Environ.*, **52**, 91 (2004).
27. S. Karmakar and H. L. Greene, *J. Catal.*, **138**, 364 (1992).
28. M. Tajima, M. Niwa, Y. Fujii, Y. Koinuma, R. Aizawa, S. Kushiyama, S. Kobayashi, K. Mizuno and H. Ohuchi, *Appl. Catal. B Environ.*, **9**, 167 (1996).
29. L. Storaro, R. Ganzerla, M. Lenarda, R. Zanoni, A. Jimenez-Lopez and P. E. Rodriguez-Castellon, *J. Mol. Catal. A Chem.*, **115**, 329 (1997).
30. P. Hoo and A. Z. Abdullah, *Korean J. Chem. Eng.*, **33**, 1200 (2016).
31. A. A. Sabri, T. M. Albayati and R. A. Alazawi, *Korean J. Chem. Eng.*, **32**, 1835 (2015).
32. S. Kawi, S. C. Shen and P. L. Chew, *J. Mater. Chem.*, **12**, 1582 (2002).
33. P. S. Chintawar and H. L. Greene, *Appl. Catal. B Environ.*, **13**, 81 (1997).
34. F. S. Xiao, Y. Han and S. L. Qiu, *Chem. J. Chin. Univ.*, **23**, 1847 (2002).
35. D. Li, Y. Zheng and X. Y. Wang, *Appl. Catal. A Gen.*, **340**, 33 (2008).
36. M. M. R. Feijen-Jeurissen, J. J. Jorna, B. E. Nieuwenhuys, G. Sinquin, C. Petit and J. P. Hindermann, *Catal. Today*, **54**, 65 (1999).
37. T. H. Ballinger and J. T. Yates, *J. Phys. Chem.*, **96**, 1417 (1992).
38. U. Beck, *Ullmann's Encyclopedia of Industrial Chemistry*, VCH Publishers, New York (1986).

Supporting Information

Effect of acid Sites on catalytic destruction of trichloroethylene over solid acid catalysts

Tiantian Wang*, Qiguang Dai,†, and Fuwu Yan*,†**

*Hubei Key Laboratory of Advanced Technology for Automotive Components & Hubei Collaborative Innovation Center for Automotive Components Technology, Wuhan University of Technology, Wuhan 430070, P. R. China
**Key Lab for Advanced Materials, Research Institute of Industrial Catalysis, School of Chemistry & Molecular Engineering, East China University of Science and Technology, Shanghai 200237, P. R. China
(*Received 5 May 2016 • accepted 24 October 2016*)

Abstract–The catalytic destruction of trichloroethylene (TCE) over several solid acid catalysts (HZSM-5, γ-Al_2O_3 and SBA-15/P) was evaluated under dry conditions. The activity order was found to be: HZSM-5>SBA-15/P>γ-Al_2O_3. It was established that Brønsted and Lewis acid sites of catalysts both played an important role on TCE catalytic destruction, but the Brønsted acid sites were more decisive. Additionally, the formation of the polychlorinated byproduct (tetrachloroethylene, PCE) over HZSM-5 and γ-Al_2O_3 catalysts was attributed to the presence of Lewis acid sites and basic O^{2-}, and PCE was not detected over SBA-15/P catalyst due to the presence of only Brønsted acid sites. The TCE/O_2-TPSR studies demonstrated that the main oxidation products formed during TCE catalytic destruction were CO, CO_2 and Cl_2, and the carbon in TCE was firstly converted to CO and then further oxidized by gas phase O_2 into CO_2.

Keywords: Trichloroethylene, CVOCs, Catalytic Oxidation, Polychlorinated Byproducts, Molecular Sieve

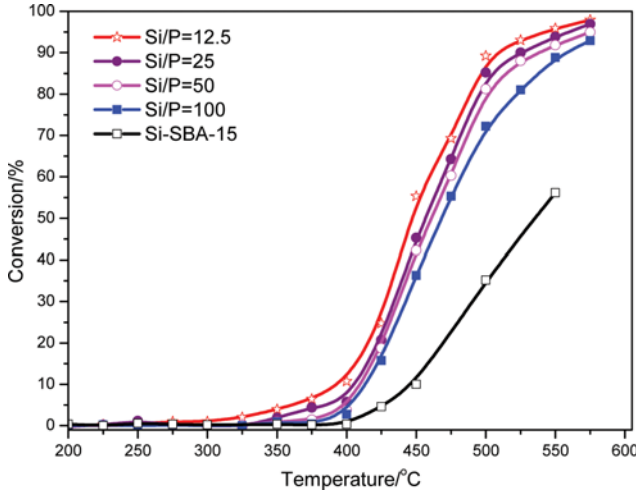

Fig. S1. Effects of Si/P ratio on catalytic activity of SBA-15/P catalyst for catalytic combustion of TCE.

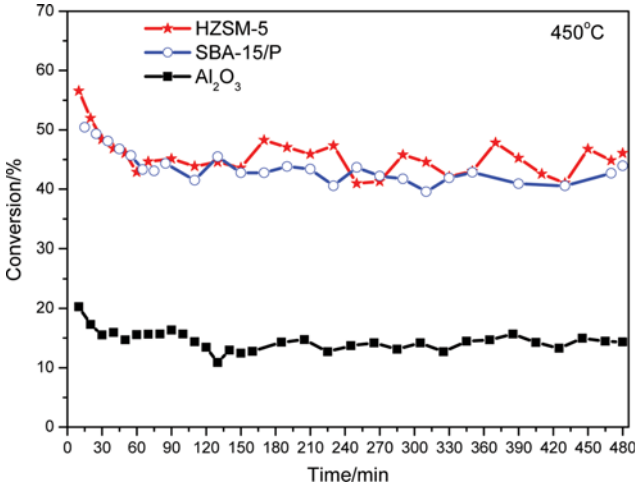

Fig. S2. The stability of catalysts for catalytic combustion of TCE.